ORIGINAL CONTRIBUTION

The collapse and aggregation of thermoresponsive poly(2-oxazoline) gradient copolymers: a time-resolved SANS study

Sebastian Jaksch · Anita Schulz · Konstantinos Kyriakos ·
Jianqi Zhang · Isabelle Grillo · Vitaliy Pipich · Rainer Jordan ·
Christine M. Papadakis

Abstract We have investigated the collapse transition of aqueous solutions of gradient copolymers from poly(*iso*-propyl-2-oxazoline)s (P*i*PrOx), which contain few hydrophobic moieties (*n*-nonyl-2-oxazoline (NOx) monomers). We extend our previous investigations (Salzinger et al., Colloid Polym Sci 290:385–400, 2012), where, for the gradient copolymers, an intermediate regime right above the cloud point was identified where small aggregates are predominant. Large aggregates are present in significant numbers only at higher temperatures. To investigate the stability of the intermediate regime, we performed time-resolved small-angle neutron scattering (SANS) experiments during temperature jumps starting below the cloud point and ending in the intermediate regime or in the high-temperature regime. We found that the intermediate regime is stable during the time investigated (~1 h). Moreover, the collapse of the small aggregates and the surface structure of the large aggregates are related to the number of hydrophobic moieties and the quench depth. The present results elucidate the structural evolution of these polymers and relate them to their final state as well as to their macroscopic behavior.

Keywords Polymer physics · Thermo-responsive polymers · Poly(2-oxazoline) · Small-angle neutron scattering · Time-resolved scattering

S. Jaksch · K. Kyriakos · J. Zhang · C. M. Papadakis (✉)
Physik-Department, Fachgebiet Physik weicher Materie, Technische Universität München, James-Franck-Str. 1, 85748 Garching, Germany
e-mail: papadakis@tum.de

A. Schulz · R. Jordan
Department Chemie, Professur für Makromolekulare Chemie, Technische Universität Dresden, Mommsenstr. 4, 01069 Dresden, Germany

I. Grillo
Large Scale Structures Group, Institut Laue-Langevin, 6, rue Jules Horowitz, 38042 Grenoble, France

S. Jaksch · V. Pipich
Jülich Centre for Neutron Science JCNS, Forschungszentrum Jülich GmbH, Outstation at MLZ, Lichtenbergstr. 1, 85748 Garching, Germany

Introduction

Thermoresponsive polymers in aqueous solution respond reversibly to small temperature stimuli by strong changes in their solubility and chain conformation, i.e., they show lower critical solution temperature (LCST) behavior [1]. Thus, they have received increased attention as smart materials, e.g., for biomedical applications [2–7] and in materials science [8–12]. Theoretical predictions for the collapse transition at the cloud point T_{CP} have been made for equilibrium conditions and have put forward the cooperativity of hydrogen bonding to the polymer as an important parameter for the nature of the transition [13]. Moreover, a number of kinetic studies during the collapse have been carried out, using time-resolved optical methods [14–18], time-resolved nuclear magnetic resonance (NMR) [19], and time-resolved light [20] as well as neutron scattering [21, 22]. Whereas some methods, such as the optical ones, feature a very high time resolution, down to the microsecond range [14], only limited by the time needed for thermal equilibration, small-angle neutron scattering (SANS) may provide detailed structural information.

Numerous works have addressed poly(*N-iso*-propyl acrylamide) (PNIPAM), which has an LCST around 31 °C [21–25]. The LCST behavior of PNIPAM has been attributed to

sequential hydrogen bond formation between PNIPAM and water [13]. PNIPAM can act both, as a H-donor and H-acceptor and can thus form intramolecular bonds [26–28]. In contrast to PNIPAM, poly(2-oxazoline) (POx; Fig. 1) is not only better suited for biomedical applications because of its excellent biocompatibility [29–33] but also because thermoresponsive poly(alkyl-2-oxazoline)s with ethyl, *iso*- or *n*-propyl side groups show a very sharp collapse transition in aqueous solution, typically within ±1 °C, and nearly no hysteresis [34, 35]. These features are attributed to the fact that POx, in contrast to PNIPAM, can only act as an acceptor when forming hydrogen bonds [36].

In contrast to, e.g., polyethers, the water-solubility of POx can be fine-tuned by the pendant 2-substitution (Fig. 1): While poly(2-methyl-2-oxazoline) (PMeOx) is highly hydrophilic, poly(2-ethyl-2-oxazoline) (PEtOx) is similarly hydrated [37] but already shows a slight amphiphilicity [38], displaying an LCST around 70 °C [39]. An additional methylene unit results in increased amphiphilicity, leading to defined cloud points of all isomers of PPrOx such as poly2-*n*-, 2-*iso*-, or 2-*cyclo*-propyl-2-oxazoline in a similar range as PNIPAM [34, 40, 41]. Even longer alkyl side groups in the homologous series of poly(2-alkyl-2-oxazoline) yield hydrophobic homopolymers. Via introduction of hydrophobic or hydrophilic 2-oxazoline moieties in poly(*iso*-propyl-2-oxazoline) (P*i*PrOx) or poly(*n*-propyl-2-oxazoline) (P*n*PrOx) such that they form gradient copolymers, the cloud point can be decreased or increased in a wide range (Fig. 1) [34, 40, 42–45].

The kinetics of the transition of thermoresponsive polymers during abrupt heating through the cloud point have been studied extensively for PNIPAM [15–19]. It was found that the collapse transition of PNIPAM is nontrivial and displays a two-step behavior: PNIPAM collapses immediately after the temperature jump, and water is expelled from the collapsed chains, which takes longer time. In previous time-resolved SANS experiments on concentrated PNIPAM solutions during a temperature jump across the cloud point, the collapse was found to be very fast, and the aggregation of the collapse comprised two steps [22]. Ye et al. [15] and Lu et al. [17] were able to detect an intermediate regime in the collapse transition of PNIPAM. We are not aware of a systematic investigation of the *kinetics* of the collapse transition of thermoresponsive poly(2-oxazoline)s. Due to the different hydrogen bonding conditions, we expect that the collapse and aggregation behavior is possibly different from the one of PNIPAM. We present here investigations of aqueous solutions of poly(2-*iso*-propyl-2-oxazoline)$_{50}$ (P*i*PrOx$_{50}$), poly[(2-*iso*-propyl-2-oxazoline)$_{48}$-(2-*n*-nonyl-2-oxazoline)$_2$]$_{grad}$ (P[*i*PrOx$_{48}$NOx$_2$]$_{grad}$) and poly[(2-*iso*-propyl-2-oxazoline)$_{46}$-(2-*n*-nonyl-2-oxazoline)$_4$]$_{grad}$ (P[*i*PrOx$_{46}$NOx$_4$]$_{grad}$) obtained by means of living cationic ring-opening polymerization. Due to their different apparent polymerization rates, the copolymerization of *iso*-propyl-2-oxazoline (k_p (80 °C)=1.25 mL/(mol s) [47] and *n*-nonyl-2-oxazoline (k_p (80 °C)=2.24 mL/(mol s) [48] yields gradient copolymers.

We have recently investigated the structural changes of similar homo- and gradient copolymers under static conditions around their respective cloud point by means of SANS [49]. The P*i*PrOx$_{50}$ homopolymer shows the expected behavior at the cloud point, namely aggregation into large aggregates due to hydrophobic interactions with the solvent, whereas the behavior of the gradient copolymers is more complex: Immediately above the cloud point, small aggregates (formed already below the cloud point) are predominant, and only at higher temperatures, large aggregates are present in significant number. The question arises, whether the small aggregates are stable with time, i.e., they will remain small, or whether, with time, large aggregates will appear at the expense of the small ones. To address this question, we have carried out time-resolved SANS investigations during temperature jumps across the cloud point. The target temperatures were chosen to be either in the intermediate regime, i.e., just above the cloud point, or in the high-temperature regime. Using D$_2$O as a solvent, the contrast in SANS was good, enabling a time resolution of 3 s. This way, we were able to follow the changes in chain conformation as well as the aggregate formation as a function of time. For the gradient copolymers, target temperatures both in the intermediate and in the high-temperature regime were chosen. For the homopolymer, no intermediate regime exists, and only one quench above the cloud point was carried out. The results reveal the influence of the amount of hydrophobic moieties and the target temperature on the chain conformation, the small aggregates, and the surface structure of the large aggregates. The present work may further improve the understanding of the pathway of the transition.
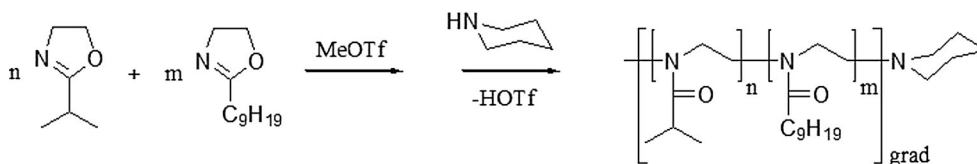
Fig. 1 Living cationic ring-opening copolymerization of *iso*-propyl-2-oxazoline and *n*-nonyl-2-oxazoline initiated with methyltriflate (*MeOTf*) and terminated with piperidine

Experimental section

Materials

All substances were purchased from Sigma-Aldrich (München, Germany) and Acros Organics (Geel, Belgium) and were used as received unless otherwise stated. Deuterated solvents for NMR analysis were obtained from Deutero GmbH (Kastellaun, Germany). NOx was received as a gift from Henkel KGaA (Düsseldorf, Germany). iPrOx was synthesized following the procedure described by Salzinger et al. [49]. All chemicals used for polymerization, methyl trifluoromethylsulfonate (MeOTf), iPrOx, NOx, chlorobenzene (ClBz), and acetonitrile (ACN) were refluxed over CaH$_2$ and distilled under nitrogen atmosphere.

Instrumentation

NMR spectra were recorded on a Bruker DRX 500 P (^{1}H, 500.13 MHz) at room temperature (RT). The spectra were calibrated to the signals of residual protonated solvent signals (CDCl$_3$, 7.26 ppm; ACN, 1.94 ppm). Gel permeation chromatography (GPC) was performed on a Polymer Laboratories GPC-120 (1× PSS GRAM analytical 1,000 and 1× PSS GRAM analytical 100; differential refractive index detector) with N,N-dimethyl acetamide (5 mmol/L LiBr, 70 °C, 1 mL/min) as eluent and polymethylmethacrylate as standards. Matrix-assisted laser desorption/ionization time-of-flight (MALDI-ToF) mass spectra were recorded on a Bruker Biflex IV (Bruker Daltonics, Bremen, Germany) using a N$_2$ laser (λ=337 nm). Microwave-supported polymerization was performed using a CEM Discover microwave oven.

Living cationic ring-opening polymerization

Under dry and inert conditions, MeOTf and monomer (s) were dissolved in 30 mL dry ACN/ClBz (50/50, v/v) at RT. The reaction mixture was irradiated in the microwave oven for 2 h with a maximum power setting of 150 W and reaction temperature of 100 °C. After cooling to RT, termination was carried out with the addition of 3 eq. piperidine and irradiation for another 60 min at 40 °C and 50 W. An excess of potassium carbonate was added, and the mixture was stirred overnight. After filtration, the mixture was concentrated, added into a mixture of chloroform and methanol (75/25, v/v), and precipitated in cold diethylether (10- to 20-fold of volume of polymer solution). After centrifugation and removal of diethylether, the precipitation was repeated one more time. The residual was dissolved in deionized water and freeze-dried. All polymers were obtained as colorless powders.

Poly(2-iso-propyl-2-oxazoline)$_{50}$ PiPrOx$_{50}$ was prepared accordingly using 436.6 mg (2.661 mmol, 1 eq.) MeOTf,

15.08 g (0.133 mol, 50 eq.) iPrOx, and 0.8 mL (8.1 mmol, 3 eq.) piperidine as terminating reagent. Yield, 9.60 g (60 %). ^{1}H-NMR (CDCl$_3$, 300 K), δ (ppm)=3.45 (br, 212H, N-CH_2CH_2); 3.07/2.97[1] (m, 2H/n.i. N-CH_3^{Ini}); 2.91–2.40 (m, 61H, CH_2^{Pid}, −CH-(CH$_3$)$_2$); 1.11 (br, 322H, −CH-(CH_3)$_2$). Polymer structure (^{1}H-NMR), PiPrOx$_{53}$. GPC (DMAc), M$_n$= 7.5 kg/mol; Đ=1.08. MALDI-ToF, M$_p$=5.7 kg/mol.

Poly[(2-iso-propyl-2-oxazoline)$_{48}$-(2-n-nonyl-2-oxazoline)$_2$]$_{grad}$ P[iPrOx$_{48}$NOx$_2$]$_{grad}$ was prepared accordingly using 422.0 mg (2.572 mmol, 1 eq.) MeOTf, 13.98 g (0.123 mol, 48 eq.) iPrOx, 1.030 g (5.220 mmol, 2 eq.) NOx, and 0.8 mL (8.1 mmol, 3 eq.) piperidine as terminating reagent. Yield, 8.1 g (59 %). ^{1}H-NMR (CDCl$_3$, 300 K), δ (ppm)=3.45 (br, 178H, N-CH_2CH_2); 3.07/2.97 (m, 2H/n.i. N-CH_3^{Ini}); 2.91–2.40 (m, 49H, CH_2^{Pid}, −CH-(CH$_3$)$_2$); 2.35 (br, 4H, CH_2-(CH$_2$)$_7$-CH$_3$); 1.56 (br, 7H, CH$_2$-CH$_2$-(CH$_2$)$_6$-CH$_3$); 1.24 (br, 29H, −CH$_2$-(CH$_2$)$_6$-CH$_3$); 1.11 (br, 259H, −CH-(CH$_3$)$_2$); 0.86 (t, 6H, −(CH$_2$)$_8$-CH$_3$). Polymer structure (^{1}H-NMR), (P[iPrOx$_{43}$NOx$_2$]$_{grad}$). GPC (DMAc), M$_n$= 7.2 kg/mol; Đ=1.07. MALDI-ToF, M$_p$=5.3 kg/mol.

Poly[(2-iso-propyl-2-oxazoline)$_{46}$-(2-n-nonyl-2-oxazoline)$_4$]$_{grad}$ P[iPrOx$_{46}$NOx$_4$]$_{grad}$ was prepared accordingly using 409.6 mg (2.496 mmol, 1 eq.) MeOTf, 13.00 g (0.115 mol, 46 eq.) iPrOx, 1.970 g (9.985 mmol, 4 eq.) NOx, and 0.8 mL (8.1 mmol, 3 eq.) piperidine as terminating reagent. Yield, 2.94 g (23 %). ^{1}H-NMR (CDCl$_3$, 300 K), δ (ppm)=3.45 (br, 169H, N-CH$_2$CH$_2$); 3.07/2.97 (m, 2H/n.i. N-CH$_3^{Ini}$); 2.91–2.41 (m, 46H, CH_2^{Pid}, −CH-(CH$_3$)$_2$); 2.34 (br, 8H, CH$_2$-(CH$_2$)$_7$-CH$_3$); 1.56 (br, 12H, CH$_2$-(CH$_2$)$_6$-CH$_3$); 1.25 (br, 49H, −CH$_2$-(CH$_2$)$_6$-CH$_3$); 1.11 (br, 230H, −CH-(CH$_3$)$_2$); 0.87 (t, 12H, −(CH$_2$)$_8$-CH$_3$). Polymer structure (^{1}H-NMR), (P[iPrOx$_{38}$NOx$_4$]$_{grad}$). GPC (DMAc), M$_n$=7.0 kg/mol; Đ=1.07.

Methods

Two weeks before the measurement, aqueous solutions of 20 mg/mL in D$_2$O (Deutero GmbH, Kastellaun, Germany) were prepared. The samples were frozen at approximately −18 °C, and then shaken at RT until they were completely molten. This procedure was repeated three times and resulted in completely transparent solutions. Until the beginning of the measurement, the samples were kept in a refrigerator (~5 °C) to avoid clouding.

---

[1] Due to restricted rotation of the methylene group, the signal is generally split into two signals (*cis/trans* position). Here, the signal at 2.97 ppm is overlapped by the multiplet of the 2-*iso*-propyl-2-oxazoline signal.

Turbidimetry

Turbidimetry was performed using a Varian Cary 50 UV–vis photo spectrometer at a wavelength of 500 nm. Temperature was increased in steps of 0.1 K with a rate of 0.1 K min^{-1}, and the cloud points of the solutions prepared as described above were determined from the decrease of the light transmission to 90 % [34, 49]. The resulting cloud point temperatures (T_{CP}) are given in Table 1. They differ slightly from the previously determined cloud points from similar polymers [49], because here freshly synthesized polymers were used. The width of the intermediate regime was assumed to be the same as previously; the resulting crossover temperatures between the intermediate and the high-temperature regime are given in Table 1.

Time-resolved SANS

SANS experiments were performed at the high-flux SANS instrument D22 at the Institut Laue-Langevin (ILL) in Grenoble, France. To enable rapid temperature changes, we used a modified Biologic SFM-300 [21]. The sample solution was equilibrated inside the reservoir for at least 15 min, while the reservoir was kept at the start temperature. The cuvette for circulating fluids (Hellma 137-QS, 1 mm thickness) was preheated to the target temperature in a custom-made sample holder. The sample was injected into the cuvette, and data acquisition was started simultaneously. During the first 2 min, the accumulation time was chosen to be 3 s, whereas it was 30 s for the subsequent 54 min. Each temperature jump was repeated at least twice for each SDD, and the resulting SANS curves were compared to ensure reproducibility. The curves were similar and were averaged to improve the statistics. The temperature profiles in the cuvettes were determined in separate measurements using a negative temperature coefficient thermistor (NTC) probe PB5-43-SD4 (Delta-R GmbH, Mannheim, Germany). These temperature profiles were used to determine the times when the cloud points were crossed. The temperature jumps envisaged for the three polymers, and the resulting start (T_{start}) and target temperatures (T_{Target}) are given in Table 2. The reservoir temperature was controlled by

a separate Julabo thermostat. We chose the reservoir temperatures close to the CP to obtain a good reproducibility of the temperature jumps, which is especially crucial when the CP is close to ambient temperature.

The neutron wavelength was $\lambda=8.0$ Å with a nominal spread of $\lambda/\lambda=10$ %, and the sample-detector distances (SDD) were 4.0 and 14.0 m. This resulted in a q range of 0.0028–0.20 Å^{-1} ($q=4\,\pi\sin(\theta/2)/\lambda$, θ is the scattering angle). A sample aperture of 6×9 mm was used. The resulting 2D images were azimuthally averaged, corrected for background scattering from both the cuvette and the solvent as well as the detector sensitivity, measured using H_2O, and brought to absolute units using the LAMP software provided by ILL giving 1D intensity curves [50].

The uncertainty in q was calculated following [50]

$$\Delta q^2 = q^2\left[\left(\frac{1}{2\sqrt{2ln2}}\frac{\Delta\lambda}{\lambda}\right)^2 + \left[\left(\frac{4\pi}{\lambda}\right)^2 - q^2\right]\Delta\theta^2 \qquad (1)$$

where the measured wavelength spread $\Delta\lambda/\lambda=13.1$ % was used. For the SDD of 4.0 m with a collimation length of 5.6 m, $\Delta\theta=1.78\times10^{-3}$ rad. In case of a SDD of 14.0 m, the collimation length was 14.4 m, which leads to $\Delta\theta=1.211\times10^{-3}$ rad (all values taken from Ref. [50]).

Modeling of SANS curves

All scattering curves show two distinct features, namely forward scattering below $q\cong0.02$ Å^{-1} due to large aggregates and the form factor scattering from single chains or small aggregates at q values above ~0.02 Å^{-1}. The curves were thus consistently modeled using

$$I(q) = I_{PL}(q) + I_{fractal}(q) + I_{bkg} \qquad (2)$$

I_{PL} denotes the forward scattering modeled by a power law, $I_{fractal}$ the scattering of single chains or small aggregates modeled by a fractal form factor, and I_{bkg} the incoherent background. These contributions are detailed below.

Single chains and small aggregates The scattering from single chains and from small aggregates was described using a form factor for small fractal objects [51]:

$$I_{fractal}(q) = I_{fractal}^0 \times \frac{1}{(qr_0)^D}\frac{D\Gamma(D-1)}{[1 + 1/(q^2\xi^2)]^{(D-1)/2}}$$
$$\times \sin[(D-1)\tan^{-1}(q\xi)] \qquad (3)$$

Here, $I_{fractal}^0$ denotes the intensity of this contribution, r_0 the radius of the building blocks constituting the fractal (see below), ξ the overall size of the chain or aggregate, Γ the gamma function, and D the fractal dimension. ξ is usually

Table 1 Cloud points and crossover temperatures between the intermediate and the high-temperature regime

	Cloud point T_{CP} (°C)	Crossover temperature (°C)[a]
PiPrOx$_{50}$	39.2[b]	–
P[iPrOx$_{48}$NOx$_2$]$_{grad}$	24.5	29.0 °C
P[iPrOx$_{46}$NOx$_4$]$_{grad}$	17.7	24.0 °C

[a] Between the intermediate and the high-temperature regime

[b] This value is consistent with the one given by Diab et al. [35], considering the difference in polymer concentration and end group

Table 2 Start and target temperatures for all jumps

	Envisaged $T_{start} \rightarrow T_{target}$ (°C)	Reservoir temperature (°C)	Measured in the cuvette (°C)[a]
PiPrOx$_{50}$	36→42	36	33.3→39.8
P[iPrOx$_{48}$NOx$_2$]$_{grad}$			
Shallow	23→27	23	24.6→27.0
Deep	23→31	23	25.2→30.0
P[iPrOx$_{46}$NOx$_4$]$_{grad}$			
Shallow	16→20	16	19.2→22.2
Deep	16→27	16	24.0→27.3

[a] For the low-start temperatures, the value of T_{start} in the cuvette is overestimated because the sample heats up already in the short hose leading from the reservoir to the cuvette

interpreted as the cutoff length of the mass fractal regime. Using this form factor instead of, e.g., the Debye form factor describing ideal chains, the expression in Eq. 3 can be used during the entire temperature jump, where the chain conformation changes from swollen to collapsed; thus, a continuous description of the chain conformation is obtained. We omit here the constant term, which is present in the fractal structure factor given originally [51], as it makes the structure factor at large q go to unity which should not be the case here. In preliminary fits, we found that r_0 varies between 6 and 7 Å for all polymers and temperature jumps. Therefore, in all further analyses, we kept r_0 constant at 6.5 Å, which corresponds to twice the monomer length a=3.7 Å [52], i.e., the persistence length, which is plausible. According to the following relation [53], D is related to the Flory exponent (ν), describing the chain conformation, by

$$\nu = \frac{3}{2+D} \tag{4}$$

Thus, the better the solvent quality, the lower the value of D: For a good solvent, ν=0.588 and D=3.10, for a θ-solvent, ν=0.5 and D=4, and for a nonsolvent, ν=0.33 and D=7.09.

Large aggregates The scattering of the large aggregates is modeled by a power law:

$$I_{PL}(q) = I_{PL}^0 q^{-\alpha} \tag{5}$$

Here, I_{PL}^0 is the intensity of the forward scattering and α the exponent of the power law. For large spheres, having a smooth interface with the solvent (i.e., the scattering length density (SLD) follows a step function from the polymer-rich aggregate to the solvent-rich matrix), α=4 [54]. Positive deviations from this behavior, i.e., values of α>4, as encountered in the present study, are due to a gradient of the SLD along the interface normal [55–57]. To estimate the gradient width, the SLD profile along the interface normal (SLD$_{grad}$(r)) is written as the convolution product of the step function describing a

smooth interface (SLD$_{smooth}$(r)) and a Gaussian function characterizing the smooth decay:

$$SLD_{grad}(r) = SLD_{smooth}(r)\exp(-\sigma^2 r^2/2) \tag{6}$$

σ^2 is the variance of the Gaussian profile and denotes the convolution product. For the scattered intensity, the following expression is obtained:

$$I_{obs}(q) = I_{Porod}^0 q^{-4} \times \exp(-\sigma^2 q^2) \tag{7}$$

To estimate σ, $\ln(I_{obs}q^4)$ was plotted vs. q^2, using the unsmeared, full-fitting curves. Strictly speaking, from this analysis, it cannot be decided whether the SLD—and thus the polymer concentration—increases from the inside toward the surface or vice versa. However, we hypothesize that it is more likely that the polymer concentration is maximum in the outer shell of the aggregate because, after the water release, a dense polymer shell is formed which may hinder residual water from the center of the aggregate to escape, thus resulting in a polymer gradient.

In most cases, the incoherent background was left as a free fitting parameter which resulted in values between 0.01 and 0.05 cm^{-1}, in accordance with the calculated value of 0.014 cm^{-1}. It turned out to be constant during all temperature jumps, i.e., the polymers did not precipitate.

All curves were analyzed using the NIST SANS package 7.04 in the IGOR Pro 6.1 environment [58] and self-written procedures.

Results

After presenting a survey of the time-resolved SANS measurements for all three polymers and the two types of temperature jump, we will discuss the homopolymer sample—which serves as a reference—and subsequently the gradient copolymers in detail. Finally, we will compare the results and discuss them.

Survey

Figure 2 shows the SANS curves taken during the temperature jumps of PiPrOx$_{50}$ and the shallow and the deep quenches of the two gradient copolymers P[iPrOx$_{48}$NOx$_2$]$_{grad}$ and P[iPrOx$_{46}$NOx$_4$]$_{grad}$, as given in Table 2. Two contributions are discerned in all scattering curves: a decay at $q>{\sim}0.02$ Å^{-1}—attributed to the scattering of single chains or small aggregates—and forward scattering at $q<{\sim}0.02$ Å^{-1} due to large aggregates. The slope of the latter increases with time, especially for PiPrOx$_{50}$ (Fig. 2a) and for the shallow quench of P[iPrOx$_{48}$NOx$_2$]$_{grad}$ (T_{Target}=27.0 °C; Fig. 2b). In the case of PiPrOx$_{50}$ (Fig. 2a) and the deep quenches of the gradient copolymers (Fig. 2d, e), the scattering due to single chains/small aggregates is relatively weak, and the large aggregates dominate, as observed by us previously [49]. Moreover, in these runs, the contribution of the small aggregates decreases with time. In the shallow quenches (Fig. 2b, c), no changes are observed in the late stages, i.e., the final state seems stable.

PiPrOx$_{50}$

The sample solution was equilibrated at the reservoir temperature of 36 °C, and its temperature increased to 39.8 °C after injection into the pre-heated cuvette (Fig. 4a). The cloud point, T_{CP}=39.2 °C, is crossed after approximately 49 s; subsequently, the temperature is stable. Representative scattering curves with fits of Eq. 2 are given in Fig. 3.

The choice of the fitting function is an important issue. In our previous work, we have chosen to model the SANS curves from PiPrOx$_{50}$ and a P[iPrOx$_{48}$NOx$_2$]$_{grad}$ solutions across the cloud point, by a Debye function, whereas the one by a P[iPrOx$_{46}$NOx$_4$]$_{grad}$ solution (all at 20 mg/mL in D$_2$O) could only be fitted by a form factor for polydisperse spheres [49]. These model functions resulted in very good and robust fits with a minimum number of parameters. Here however, the resulting chain radii could not easily be compared as the inner structures of a compact sphere and a Gaussian chain are different. Therefore, we chose a different approach here. To compare the chain conformations of the polymers with each other and to characterize their changes across the cloud point, we describe them as fractals with a cutoff length. This way, good fits were obtained for all polymers and all temperatures (Fig. 3). The form factor of a small fractal is thus appropriate to describe the initially molecularly dissolved chains; and, moreover, the change in chain conformation during the collapse is also captured. To model the scattering caused by large aggregates, we chose in our previous work to use a model function for large spheres. Here, we decided to use a modified Porod law instead, because the forward scattering follows a power law in all cases, the aggregate radius cannot be determined reliably because of the limited q range, and we strive at using as few fitting parameters as possible. Below, we compare the results of the two ways of fitting.

Results of the fits of Eq. 2 are compiled in Fig. 4. During the first 45 s, the forward scattering intensity I_{PL}^0 decays by five orders of magnitude (Fig. 4b), and the exponent α increases from 3.1 to 5.4, then both values remain constant. Thus, the aggregate surface is first fractal ($\alpha<4$), and with time, a surface gradient develops ($\alpha>4$). At the end of the run, the gradient width is $\sigma = 135\pm7$ Å (Eq. 7), i.e., significantly larger than a single chain, see below. We note that the decay in the measured scattering curve appears to have a slope close to 4, however, due to smearing with the resolution function, the true value of α is larger.

The intensity of the contribution from single chains, $I_{fractal}^0$, scatters around a value of 0.025 cm^{-1} and eventually reaches 0.02 cm^{-1} (Fig. 4c). D decreases within the first 24 s from 3.6 ±1.3 to 2.8±0.3 (Fig. 4d), which corresponds to an increase of v from 0.53±0.12 to v=0.63±0.04. The initial and the final values are slightly lower and slightly higher than the value expected for a polymer in a good solvent, v=0.588, respectively. The aggregate size, i.e., the upper cutoff length of the fractal (ξ) is initially 9±4 Å, which is in consistency with the results obtained by Ye et al. [46]. These authors found for poly(ethyl-2-oxazoline) unimers the relation R_h=0.179 Å× $M_w^{0.539}$. Accounting for the difference in molar masses, we expect R_h=0.179 Å×$(M_w/1.37)^{0.539}$ for PiPrOx. Using the relationship R_g=0.775×R_h [59] for polymers, the radius of gyration of PiPrOx is estimated at R_g=14.4 Å [59]. This number is within the same range as the ξ value obtained by us; therefore, we conclude that, far below the cloud point, most polymers are present as unimers. As time proceeds, ξ increases, until it reaches a value of 19±7 Å 30 s after the injection, before decreasing to a final value of 13.0±1.7 Å. This increase and subsequent decrease may be attributed to the transient aggregation of a few chains: Small aggregates are formed already below T_{CP} and collapse above.

We conclude that the PiPOx$_{50}$ homopolymers are molecularly dissolved far below T_{CP}. As T_{CP} is approached, small aggregates form which shrink as T_{CP} is passed, in consistency with our previous observations in temperature-resolved experiments [49]. Above T_{CP}, additional large aggregates are formed featuring an initially smooth surface which changes into a concentration gradient at later times. This may be due to a depletion of solvent (D$_2$O) in the near-surface region, which may hinder further growth of the aggregates, as found in previous work on PNIPAM [60–63].

P[iPrOx$_{48}$NOx$_2$]$_{grad}$—shallow quench

For P[iPrOx$_{48}$NOx$_2$]$_{grad}$, we performed a shallow quench from 23.0 to 27.0 °C, i.e., into the intermediate regime (Fig. 2b). The cloud point of T_{CP}=24.5 °C was reached immediately after injection, and the temperature becomes stable at 27.0 °C after ~100 s (Fig. 5a). As for PiPrOx$_{50}$,
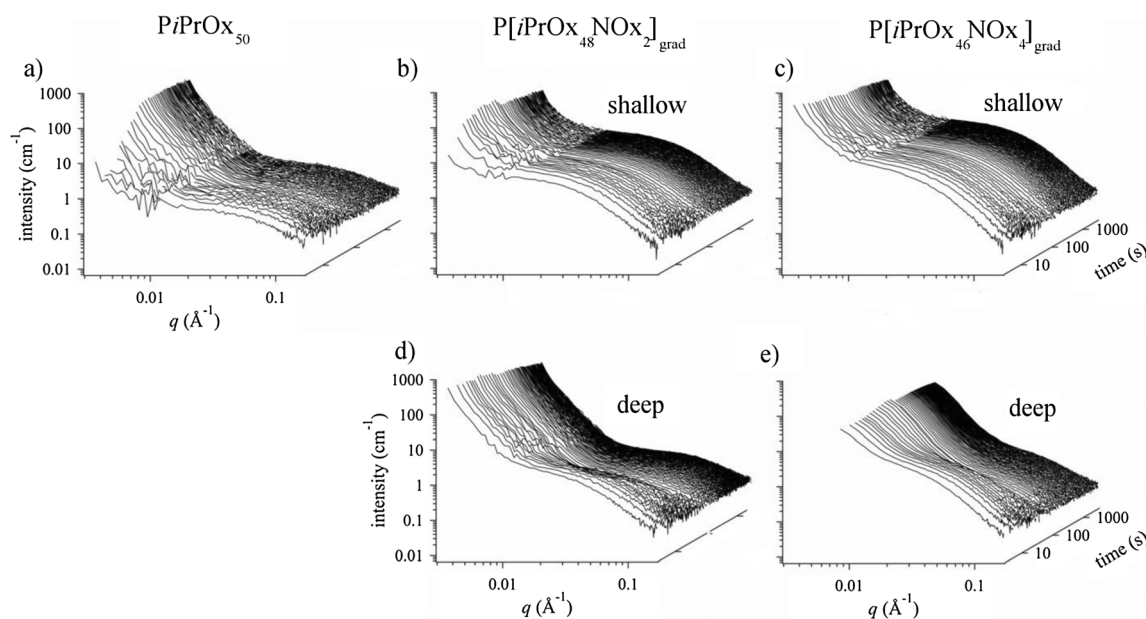
Fig. 2 SANS curves taken during the temperature jumps. **a** PiPrOx$_{50}$, T_{Target}=39.8 °C. **b, d** P[iPrOx$_{48}$NOx$_2$]$_{grad}$, T_{Target}=27.0 °C (**b**) and 30.0 °C (**d**). **c, e** P[iPrOx$_{46}$NOx$_4$]$_{grad}$, T_{Target}=22.2 °C (**c**) and 27.3 °C (**e**)

two regimes are distinguished: Initially, the slope of the forward scattering increases; then, it stays constant.

The results of the fits of Eq. 2 to the curves are shown in Fig. 5b–e. The prefactor of the forward scattering (I^0_{PL}) decreases steadily over the entire measurement time. The exponent α increases during the first 21 s from 4.2 to 5.6, i.e., the initially smooth surface of the large aggregates develops a concentration gradient. Later, no more change is observed. The final gradient width is σ =247±9 Å.

The fractal prefactor $I^0_{fractal}$ decreases slightly during the first 60 s and more strongly during the subsequent 30 s, then, it becomes constant. The fractal dimension, D, is constant at 3.1-3.2, which corresponds to a Flory exponent ν =0.58–0.59, i.e., the solvent is good. The size ξ is initially 24.2±1.5 Å. This value is higher than the one of the PiPrOx$_{50}$ homopolymers (9 ±4 Å); thus, P[iPrOx$_{48}$NOx$_2$]$_{grad}$ forms small aggregates already below the cloud point because of intermolecular

bridging by the hydrophobic n-nonyl groups of the NOx monomers [47]. ξ decreases to 21.8±0.7 Å during the first 66 s and during the subsequent 60 s to 19.3±0.7 Å, which reflects the collapse of the small aggregates.

We conclude that the large aggregates behave in the same way as for PiPrOx$_{50}$. The solvent quality is slightly worse than for PiPrOx$_{50}$, as expected. Instead of single chains, small aggregates are present which collapse during the temperature jump. All fit parameters reach stable values after 100 s, i.e. when the cuvette reaches the target temperature. There seems to be no delay once T_{CP} is crossed.

P[iPrOx$_{48}$NOx$_2$]$_{grad}$—deep quench

When quenching P[iPrOx$_{48}$NOx$_2$]$_{grad}$ from 23.0 to 30.0 °C, i.e., high above the cloud point, T_{CP}=24.5°C was reached immediately after the injection (Fig. 5f). Two regimes are distinguished (Fig. 2d): While the forward scattering stays nearly unchanged during the entire run, the decay at high q values (q>0.02 Å^{-1}) changes shape during the first 100 s. Later, no more changes are observed.

The fitting results are compiled in Fig. 5g–j. The prefactor I^0_{PL} and the exponent α are nearly constant. α decreases from α=5.6±0.1 to α=5.4±0.1 during the first 60 s and then stays constant. Thus, a surface gradient is already present from the beginning of the measurements, i.e., the early stage is missed. The final gradient width σ is 140±7 Å.

The fractal prefactor decreases during the first 120 s and then stays constant. D is constant at 3.1±0.1 during the first 30 s, then it increases and reaches 3.5±0.7 110 s after the injection, i.e., ν decreases from 0.59±0.01 to 0.54±0.07. The initially good solvent thus becomes slightly worse but not yet
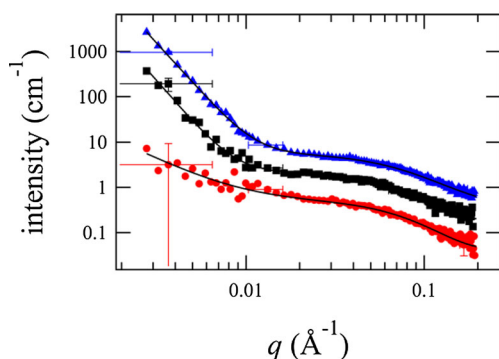
Fig. 3 Representative scattering curves from PiPrOx$_{50}$ at 6 s (*red circles*), 48 s (*black squares*), and 3,360 s (*blue triangles*) after the injection. The *solid lines* are fits of Eq. 2. The curves were shifted vertically for clarity
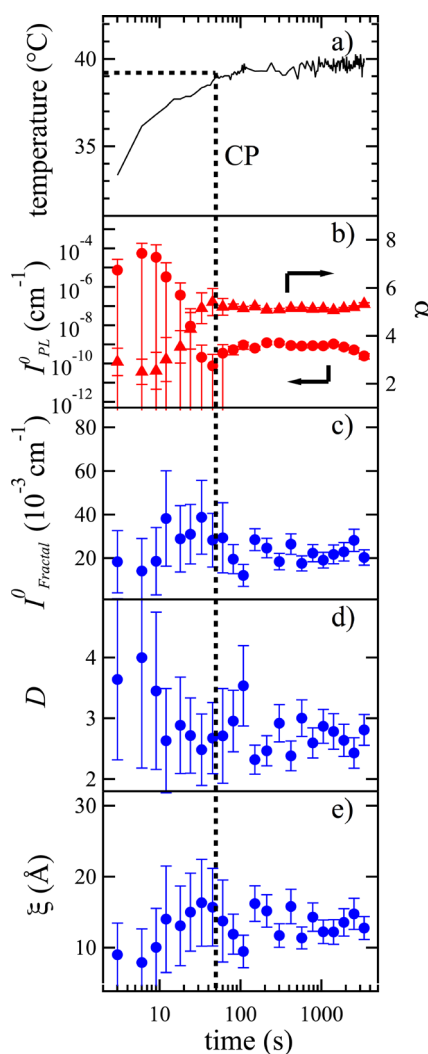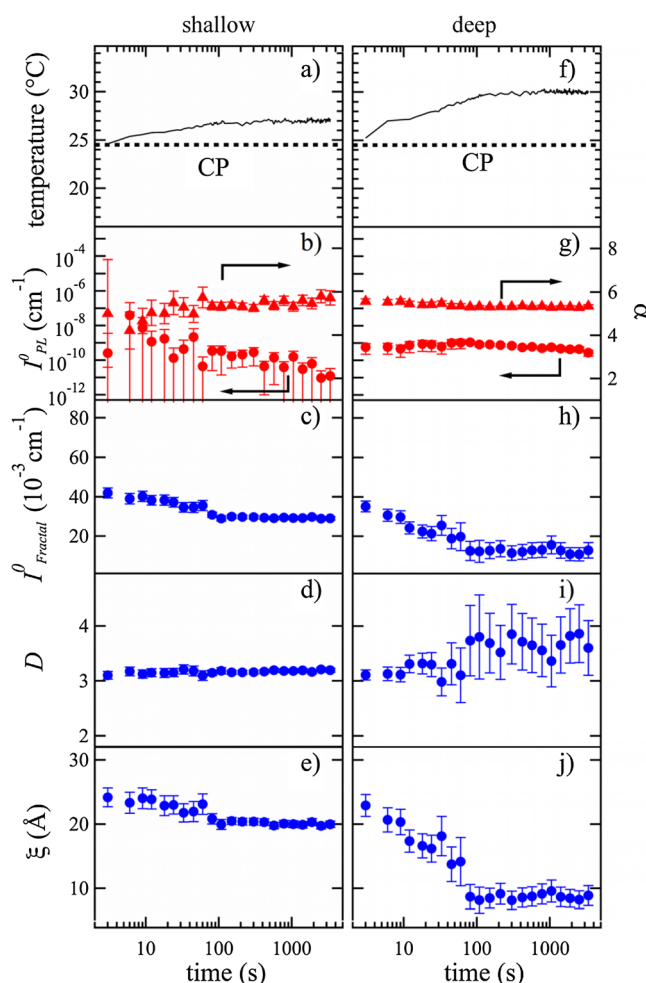
Fig. 4 Temperature jump of P*i*PrOx50 from 36.0 to 39.8 °C. Temperature profile (**a**) and results of fits from Eq. 2 (**b**–**e**). *Red symbols* in (**b**) are calculated using the scaling law for the forward scattering, *blue symbols* in (**c**–**e**) are calculated using the fractal form factor. The *vertical dashed line* indicates the time when T_{CP} is crossed. **a** Prefactor of the forward scattering. **b** Exponent α (*triangles*), prefactor $I^0_{fractal}$ (*circles*). **c** Fractal dimension D (**d**) and size of the small aggregates ξ (**e**). The *arrows* in (**b**) indicate the axis used for the respective values. For better visibility, data points at later times are omitted

Fig. 5 Shallow (*left*) and deep quench (*right*) of P[*i*PrOx$_{48}$NOx$_2$]$_{grad}$. Same notations and symbols as in Fig. 4. The *arrows* in (**b, g**) indicate the axis used for the respective values. For better visibility, data points at later times are omitted

a theta solvent. The final solvent quality is worse than in the end of the shallow quench of the same polymer, as expected. ξ decreases from 23±2 to 8±2 Å 110 s after the injection, i.e., the small aggregates collapse. This means the collapse is stronger than for the shallow quench and the solvent quality becomes worse.

P[*i*PrOx$_{46}$NOx$_4$]$_{grad}$—shallow quench

In the shallow quench of the P[*i*PrOx$_{46}$NOx$_4$]$_{grad}$ solution, the temperature was changed from 16.0 to 22.2 °C (Fig. 6a). The cloud point, T_{CP}=17.7 °C, was reached immediately after injection, and the temperature became constant after ~150 s.

The SANS curves do not show any obvious changes (Fig. 2c). The fitting results are compiled in Fig. 6b–e. Whereas the prefactor of the forward scattering decreases slightly over the entire measurement time, the exponent α increases from 5.2±0.2 to 5.6±0.2. Thus, the surface gradient is already present at the beginning of the measurement. The final gradient width is σ =228±10 Å.

The prefactor of the small aggregates decreases slightly during the first 60 s, then more strongly until 100 s after injection, and eventually it is constant. D is nearly constant at 3.10–3.25, which corresponds to a value between ν=0.588 and ν=0.571, i.e., a good solvent. ξ decreases slightly from 27±1 to 23±1 Å during the first 60 s, then more strongly to ξ= 20.6±0.4 Å 100 s after the injection where it remains. Thus, small aggregates are initially present which collapse as the cloud point is crossed.

The main structural change in this temperature jump is the collapse of the small aggregates.

P[iPrOx$_{46}$NOx$_4$]$_{grad}$—deep quench

In the deep quench, temperature was changed from 16.0 to 27.2 °C. Again, T_{CP}=17.7 °C was reached immediately after injection, and temperature became constant after ~130 s. Due to the limited beam time, we could only measure at a SDD of 4.0 m, i.e., in the limited q range of 0.01–0.2 Å^{-1}. The forward scattering could thus not be resolved properly. The time series (Fig. 2e) displays again two regimes: During the first 80 s, the intensity in the range $q>0.02$ Å^{-1} changes shape, then remains unchanged.

Results of the fits of Eq. 2 to the curves are seen in Fig. 6g–j. The prefactor and exponent of the forward scattering cannot be determined reliably, and we therefore do not discuss them further. The prefactor of the small aggregates decreases during the first 100 s and then remains constant. D is 3.1–3.2 throughout the measuring time, which corresponds to values ν=0.58–

0.59 and ν=0.58, i.e., the solvent is good. ξ has an initial value of 25±3 Å; it decreases during the first 100 s to 17±5 Å and during the subsequent 50 s to 13±2 Å. This initial aggregate size is comparable to the value for the shallow jump, as expected because the initial conditions are the same, whereas the collapse, as for P[iPrOx$_{48}$NOx$_2$]$_{grad}$ is more pronounced for the deep quench.

Discussion

We have followed the structural changes of aqueous solutions of the homopolymer PiPrOx$_{50}$ and the gradient copolymers P[iPrOx$_{48}$NOx$_2$]$_{grad}$ and P[iPrOx$_{46}$NOx$_4$]$_{grad}$ during temperature jumps across the cloud point, i.e., from the swollen to the collapsed state. For the gradient copolymers, the temperature jumps were performed both into the intermediate state and into the high-temperature regime. Time-resolved SANS with a time resolution of 3 s allowed us to follow the evolution of (i) the single chains/small aggregates with respect to the aggregate size and the chain conformation and (ii) the presence and the surface structure of the large aggregates. All solutions reach equilibrium latest after 150 s, and no further changes were observed during the remaining time (~1 h); thus, on this time scale, the intermediate regime is stable.

The initial and final values of the most important characteristics are compiled in Fig. 7. The initial values of the correlation lengths of the unimers (Fig. 7a) show that the homopolymer PiPrOx$_{50}$ is initially present as unimers, whereas the gradient copolymers form small aggregates because of intermolecular interaction due to the n-nonyl side groups. Thus, the inclusion of NOx monomers promotes aggregation. The final aggregate size (ξ) of PiPrOx$_{50}$ is higher than the initial one, which is a consequence of the aggregation accompanying the collapse of the unimers. For the gradient copolymers, the final correlation lengths are consistently lower than the initial ones. As expected, for the deep quenches into the high-temperature regime, the collapse is stronger than for the shallow ones into the intermediate regime.
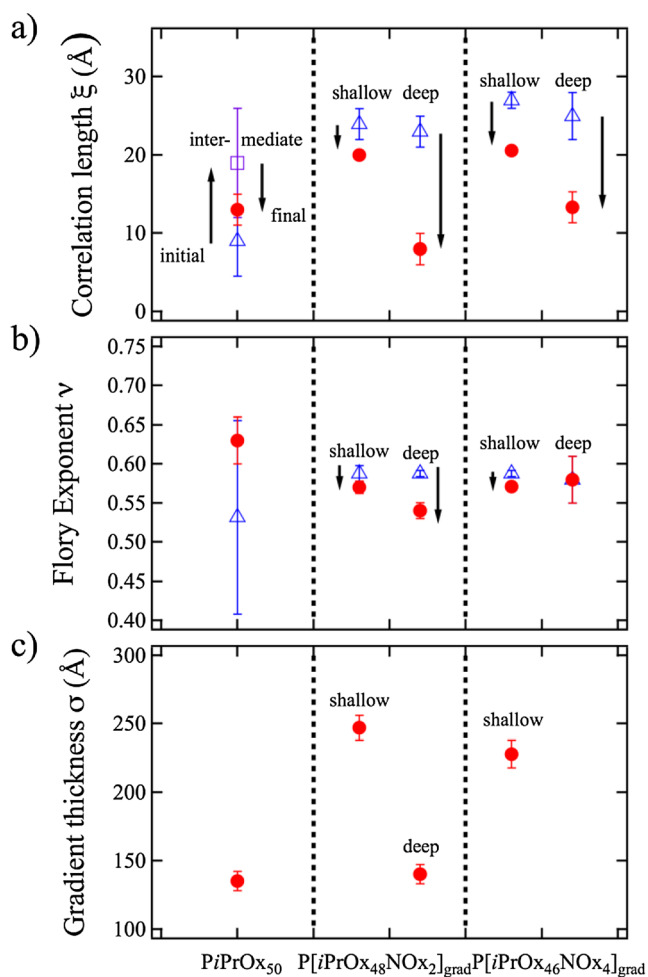
This intermediate regime found by us compares to the intermediate regimes found for PNIPAM by Ye et al. [15] and Lu et al. [17]. In the PNIPAM system, however, the intermediate regime is a transient phenomenon and, after an equilibration time, the chains collapse fully. In the present case, the strength of the collapse seems to be solely related to the target temperature, and the chain conformation does not change further with time after the initial collapse.

Fitting a form factor for small fractal aggregates formed by the monomers allowed us to characterize the scattering from the single chains/small aggregates by fitting the same expression throughout, both in the swollen and the collapsed state. Our aim was to characterize the chain conformation as a
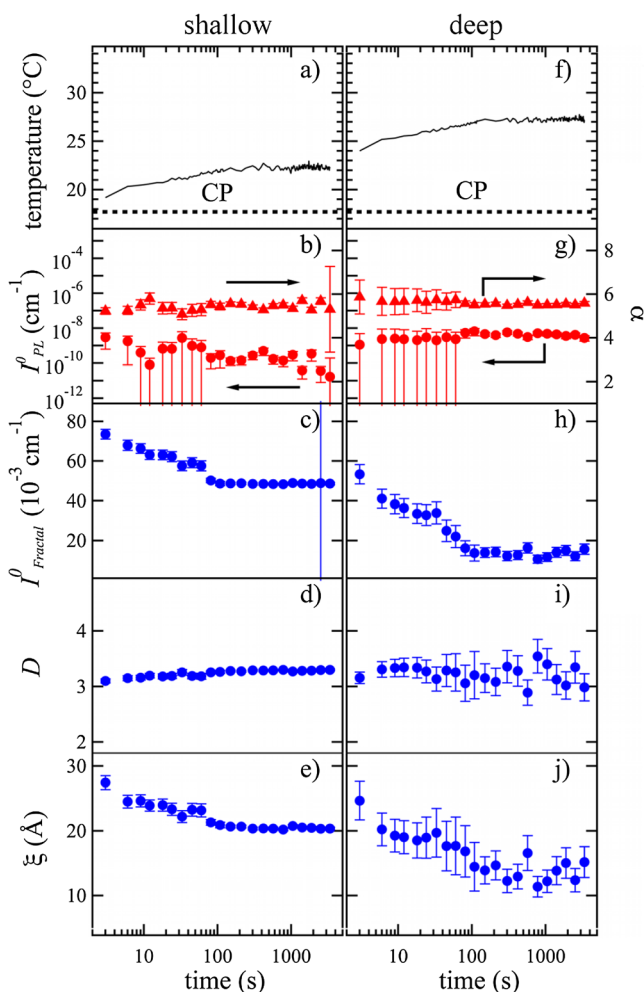
Fig. 6 Shallow (*left*) and deep quench (*right*) of P[iPrOx$_{46}$NOx$_4$]$_{grad}$. Same notations and symbols as in Fig. 4. The values in (**g**) suffer from large uncertainties due to the limited q range. The *arrows* in (**b**, **g**) indicate the axis used for the respective values. For better visibility, data points at later times are omitted

function of time and temperature across T_{CP}, in the intermediate and the high-temperature regime. The values of the Flory exponent ν seem to be slightly overestimated, but the trend upon collapse in dependence of the depth of the quench is recovered (Fig. 7b). The reason may be 2-fold: First, the prefactor of the forward scattering and the slope of the forward scattering are strongly correlated parameters. Second, the fractal dimension is only obtained from the decay of the scattering curves in the high q region ($q > 0.06$ Å^{-1}). This contribution is in many cases very low, especially above T_{CP} where only few chains are still molecularly dissolved and possibly more swollen than those (the majority), which are located in the large aggregates. The qualitative behavior, however, confirms the expectations for the collapse of a thermoresponsive polymer: The higher the content of hydrophobic moieties, the worse is the solvent quality. The same
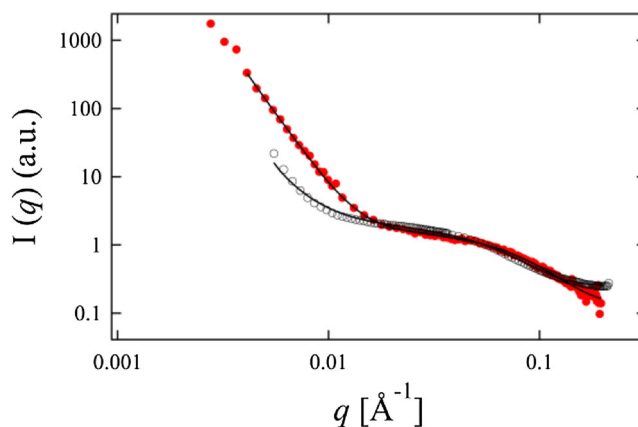
holds for the final states of the quenches to high temperatures where the polymer is more hydrophobic.

The exponent describing the slope of the forward scattering, α, gives information about the surface structure of the large aggregates. We found $\alpha > 4$ for all polymers at all target temperatures, i.e., the final state of the aggregates seems to feature a concentration gradient along the surface normal. For the homopolymer, α increases with time: The aggregate surface is initially rough, then it becomes smooth, and a surface gradient having a width of 135 Å appears (Fig. 7c). A similar gradient width is found for the gradient copolymer $P[iPrOx_{48}NOx_2]_{grad}$ at the end of the deep quench. For the shallow jumps, much higher values (~200–250 Å) are encountered for both gradient copolymers. Additional USANS measurements (Fig. S1 in the Supporting Information) revealed that the aggregate have radii of $R \cong 6000$ Å, i.e., the concentration gradient is a surface effect. It can either be attributed to the release of D_2O from the surfaces resulting in a dense surface layer at the surface or to the swelling of the surface-near region with D_2O. In PNIPAM homopolymers, no concentration gradient was detected [22]. However, the surface structure may not only depend on the chemical nature of the polymer, but also on the polymer concentration and the details of the temperature jump.

Comparison with previous results

To compare the present results from time-resolved measurements during temperature jumps with our previous static, temperature-resolved investigation [49], we reevaluated these static curves using Eq. 2. Representative curves from

Fig. 7 Initial and final values of **a** the correlation length of the single chains/small aggregates (ξ), **b** the Flory exponent (ν), and **c** the width of the surface gradient of the large aggregates (σ). *Open blue triangles*, initial values; *purple square*, value at the cloud point; *closed red circles*, final values. *Arrows* indicate the time-dependent behavior. The *vertical dashed lines* separate the samples from each other

Fig. 8 Scattering curves from $P[iPrOx_{48}NOx_2]_{grad}$ from the static temperature-resolved measurement at 30.7 °C (*open black circles*) [49] and the data for 720 s after the jump of the time-resolved measurement (*red dots*) for $P[iPrOx_{48}NOx_2]_{grad}$ from the deep temperature jump from 23.0 to 30.0 °C (Fig. 5f–j). Both curves were measured at least 12 min after crossing T_{CP} and at a temperature of 5.6 K above T_{CP}. For better visual comparison, the curve from the temperature jump was shifted to match the static measurement
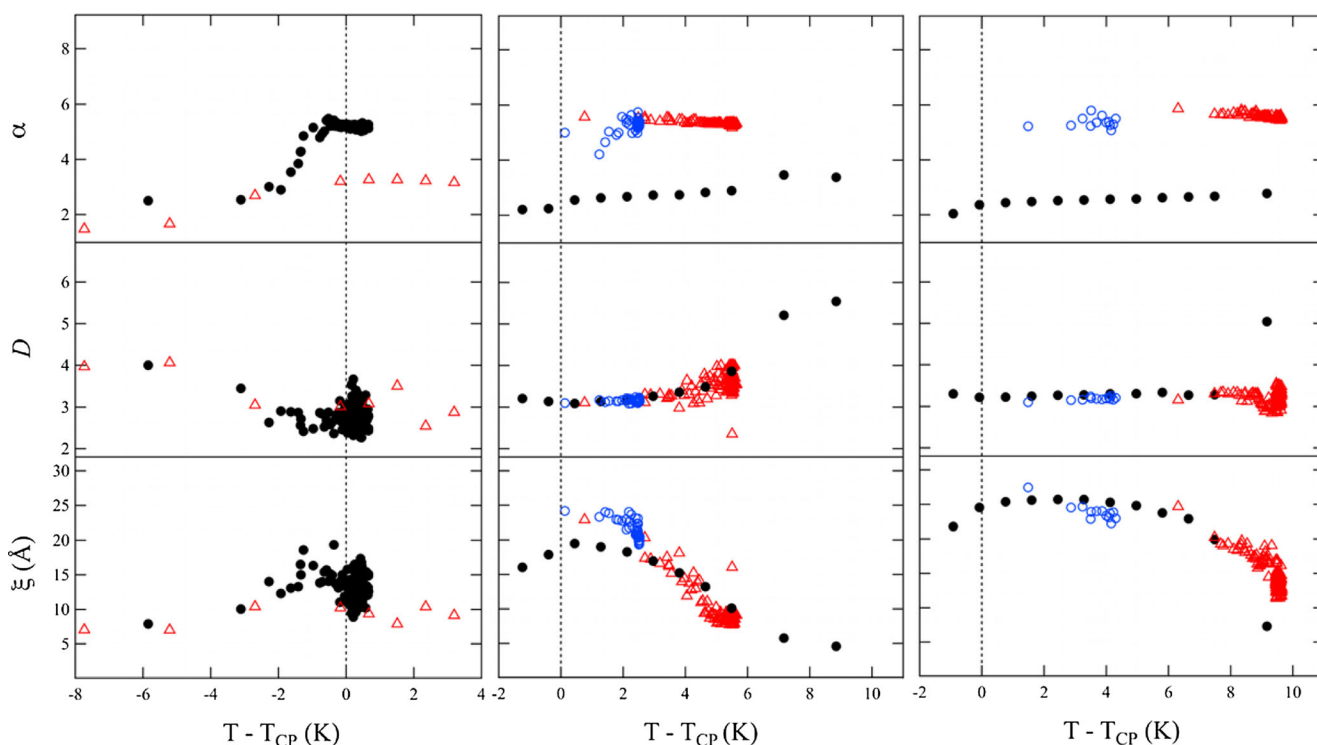
Fig. 9 Parameters from fits of Eq. 2 to the static curves (*closed black circles*) [49] and the curves from the temperature jumps: shallow quenches (*open blue circles*) and deep quenches (*open red triangles*), in P[*i*PrOx$_{48}$NOx$_2$]$_{grad}$ at 20 mg/mL in D$_2$O are shown in Fig. 8 together with the fits. The minimum q value in the present study is with ~2×10^{-3} Å^{-1} lower than in our previous study (5×10^{-3} Å^{-1}). Also, the signal-to-noise ratio is improved. Thus, the fitting parameters obtained for the forward scattering cannot be directly compared. However, this does not affect the data collected at higher q values where information about the single chains/small aggregates is found. The resulting fitting parameters from the static and the time-resolved data sets are shown in Fig. 9 in dependence on the temperature difference to T_{CP}. While the discrepancy for α is probably due to the difference in q range as well as the different settings, the values of D and ξ coincide very well for the static data and the deep quenches. This corroborates the existence of the intermediate regime and that the final chain conformation only depends on the final temperature.

dependence on temperature difference to T_{CP}. The data are given for P*i*PrOx$_{50}$ (*left*), P[*i*PrOx$_{48}$NOx$_2$]$_{grad}$ (*middle*), and P[*i*PrOx$_{46}$NOx$_4$]$_{grad}$ (*right*). *Vertical dashed lines* mark the temperature of the cloud point T_{CP}

hydrophobic moieties. Deeper quenches result in a stronger collapse of the small aggregates at T_{CP} and in thinner surface gradient layers of the large aggregates. Comparison with the static results shows good coincidence, which justifies the use of the finite fractals as a model function describing the chain size and conformation.

Time-resolved structural investigations of the phase separation at T_{CP} of aqueous solutions of thermoresponsive polymers are still scarce. A recent study addresses aqueous solutions of a concentrated PNIPAM homopolymer where a very deep quench into the phase-separated regime was carried out [22]. Our finding of a finite surface gradient in the P*i*PrOx$_{50}$ homopolymer differs from the smooth surface observed in the PNIPAM solution. Moreover, the two-step behavior encountered with PNIPAM could not be detected in the present P*i*PrOx system. A possible reason is the different nature of the binding of water to the polymers and its release. By being able to form hydrogen bonds with itself, PNIPAM can expel the water to a higher degree than in the case of POx, which does not form hydrogen bonds with itself. This leads to remaining solvent within the POx aggregates, which then causes the observed surface gradient.

Conclusions

In the present study, we confirm that the gradient copolymers form small aggregates already below T_{CP}. Moreover, the intermediate regime found in our previous work is stable [49]. Comparing different jump depths allows us to determine the influence of the quench depth in gradient copolymers differing in the amount of

References

1. Aseyev VO, Tenhu H, Winnik FM (2006) Temperature dependence of the colloidal stability of neutral amphiphilic polymers in water. In: Khokhlov AR (ed) Conformation-dependent design of sequences in copolymers, vol 196, Advances in Polymer Science. Springer-Verlag Berlin, Berlin, pp 1–85

2. Hoffman AS (1987) Applications of thermally reversible polymers and hydrogels in therapeutics and diagnostics. J Control Release 6: 297–306

3. Cammas S, Suzuki K, Sone C, Sakurai Y, Kataoka K, Okano T (1997) Thermo-responsive polymer nanoparticles with a core-shell micelle structure as site-specific drug carriers. J Control Release 48:157–164

4. Coughlan DC, Quilty FP, Corrigan OI (2004) Effect of drug physicochemical properties on swelling/deswelling kinetics and pulsatile drug release from thermoresponsive poly(N-isopropylacrylamide) hydrogels. J Control Release 98:97–114

5. Schmaljohann D (2006) Thermo- and pH-responsive polymers in drug delivery. Adv Drug Deliv Rev 58:1655–1670

6. Hoogenboom R, Schlaad H (2011) Bioinspired poly(2-oxazoline)s. Polymers 3:467–488

7. Sedlacek O, Monnery BD, Filippov SK, Hoogenboom R, Hruby M (2012) Poly(2-oxazoline)s—are they more advantageous for biomedical applications than other polymers? Macromol Rapid Commun 33: 1648–1662

8. Bartel W (1982) Temperature-dependent control element. Germany Patent DE3223771-A,

9. Kishi R, Hara M, Sawahata K, Osada Y (1991) Conversion of chemical into mechanical energy by synthetic-polymer gels (chemomechanical system). Fundamentals and Biomedical Applications. Plenum Press Div Plenum Publishing Corp, New York, Polymer Gels

10. Peters EC, Svec F, Fréchet JMJ (1997) Thermally responsive rigid polymer monoliths. Adv Mater 9:630–633

11. Arndt KF, Kuckling D, Richter A (2000) Application of sensitive hydrogels in flow control. Polym Adv Technol 11:496–505

12. Nykänen A, Nuopponen M, Laukkanen A, Hirvonen SP, Rytelä M, Turunen O, Tenhu H, Mezzenga R, Ikkala O, Ruokolainen J (2007) Phase behavior and temperature-responsive molecular filters based on self-assembly of polystyrene-block-poly(N-isopropylacrylamide)-block-polystyrene. Macromolecules 40:5827–5834

13. Okada Y, Tanaka F (2005) Cooperative hydration, chain collapse, and flat LCST behavior in aqueous poly(N-isopropylacrylamide) solutions. Macromolecules 38:4465–4471

14. Wang J, Gan D, Lyon LA, El-Sayed MA (2001) Temperature-jump investigations of the kinetics of hydrogel nanoparticle volume phase transitions. J Am Chem Soc 123:11284–11289

15. Ye X, Lu Y, Shen L, Ding Y, Liu S, Zhang G, Wu C (2007) How many stages in the coil-to-globule transition of linear homopolymer chains in a dilute solution? Macromolecules 40:4750–4752

16. Tsuboi Y, Yoshida Y, Kitamura N, Iwai K (2009) Phase transition dynamics of fluorescent-labeled poly(N-isopropylacrylamide) in aqueous solution as revealed by time-resolved spectroscopy combined with a laser T-jump technique. Chem Phys Lett 468:42–45

17. Lu Y, Ye X, Li J, Li C, Liu S (2011) Kinetics of laser-heating-induced phase transition of poly(N-isopropylacrylamide) chains in dilute and semidilute solutions. J Phys Chem B 115:12001–12006

18. Inoue H, Kuwahara S, Katayama K (2013) The whole process of phase transition and relaxation of poly(N-isopropylacrylamide) aqueous solution. Phys Chem Chem Phys 15:3814–3819

19. Yushmanov PV, Furó I, Iliopoulos I (2006) Kinetics of demixing and remixing transitions in aqueous solutions of poly(N-isopropylacrylamide): a temperature-jump 1H NMR study. Macromol Chem Phys 207:1972–1979

20. Takahashi R, Sato T, Terao K, Qiu XP, Winnik FM (2012) Self-association of a thermosensitive poly(alkyl-2-oxazoline) block copolymer in aqueous solution. Macromolecules 45:6111–6119

21. Adelsberger J, Metwalli E, Diethert A, Grillo I, Bivigou-Koumba AM, Laschewsky A, Müller-Buschbaum P, Papadakis CM (2012) Kinetics of collapse transition and cluster formation in a thermoresponsive micellar solution of P (S-b-NIPAM-b-S) induced by a temperature jump. Macromol Rapid Commun 33:254–259

22. Meier-Koll A, Pipich V, Busch P, Papadakis CM, Müller-Buschbaum P (2012) Phase separation in semidilute aqueous poly(N-isopropylacrylamide) solutions. Langmuir 28:8791–8798

23. Heskins M, Guillet JE (1968) Solution properties of poly(N-isopropylacrylamide). Journal of Macromolecular Science: Part A — Chemistry 2:1441–1455

24. Winnik FM (1990) Phase-transition of aqueous poly-(N-isopropylacrylamide) solutions—a study by nonradiative energy-transfer. Polymer 31:2125–2134

25. Afroze F, Nies E, Berghmans H (2000) Phase transitions in the system poly(N-isopropylacrylamide)/water and swelling behaviour of the corresponding networks. J Mol Struct 554:55–68

26. Shan-Yang L, Ko-Shao C, Liang R-C (1999) Thermal micro ATR/FT-IR spectroscopic system for quantitative study of the molecular structure of poly(N-isopropylacrylamide) in water. Polymer 40: 2619–26242624

27. Katsumoto Y, Tanaka T, Sato H, Ozaki Y (2002) Conformational change of poly(N-isopropylacrylamide) during the coil-globule transition investigated by attenuated total reflection/infrared spectroscopy and density functional theory calculation. J Phys Chem A 106:3429–3435

28. Zhou KJ, Lu YJ, Li JF, Shen L, Zhang GZ, Xie ZW, Wu C (2008) The coil-to-globule-to-coil transition of linear polymer chains in dilute aqueous solutions: effect of intrachain hydrogen bonding. Macromolecules 41:8927–8931

29. Gaertner FC, Luxenhofer R, Blechert B, Jordan R, Essler M (2007) Synthesis, biodistribution and excretion of radiolabeled poly(2-alkyl-2-oxazoline)s. J Control Release 119:291–300

30. Adams N, Schubert US (2007) Poly(2-oxazolines) in biological and biomedical application contexts. Adv Drug Deliv Rev 59:1504–1520

31. Han YC, He ZJ, Schulz A, Bronich TK, Jordan R, Luxenhofer R, Kabanov AV (2012) Synergistic combinations of multiple chemotherapeutic agents in high capacity poly(2-oxazoline) micelles. Mol Pharm 9:2302–2313

32. Luxenhofer R, Han Y, Schulz A, Tong J, He Z, Kabanov AV, Jordan R (2012) Poly(2-oxazoline) s as polymer therapeutics. Macromol Rapid Commun 33:1613–1631

33. Zhang N, Pompe T, Amin I, Luxenhofer R, Werner C, Jordan R (2012) Tailored poly(2-oxazoline) polymer brushes to control protein adsorption and cell adhesion. Macromol Biosci 12:926–936

34. Huber S, Jordan R (2008) Modulation of the lower critical solution temperature of 2-alkyl-2-oxazoline copolymers. Colloid Polym Sci 286:395–402

35. Diab C, Akiyama Y, Kataoka K, Winnik FM (2004) Microcalorimetric study of the temperature-induced phase separation in aqueous solutions of poly(2-isopropyl-2-oxazolines). Macromolecules 37:2556–2562

36. Maeda Y, Sakamoto J, Wang SY, Mizuno Y (2009) Lower critical solution temperature behavior of poly(N-(2-ethoxyethyl) acrylamide) as compared with poly(N-isopropylacrylamide). J Phys Chem B 113: 12456–12461

37. Rehfeldt F, Tanaka M, Pagnoni L, Jordan R (2002) Static and dynamic swelling of grafted poly(2-alkyl-2-oxazoline)s. Langmuir 18:4908–4914

38. Foreman MB, Coffman JP, Murcia MJ, Cesana S, Jordan R, Smith GS, Naumann CA (2003) Gelation of amphiphilic lipopolymers at the air-water interface: 2D analogue to 3D gelation of colloidal systems with grafted polymer chains? Langmuir 19:326–332

39. Lin PY, Clash C, Pearce EM, Kwei TK, Aponte MA (1988) Solubility and miscibility of poly(ethyl-oxazoline). J Polym Sci Pt B-Polym Phys 26:603–619

40. Park JS, Kataoka K (2007) Comprehensive and accurate control of thermosensitivity of poly(2-alkyl-2-oxazoline)s via well-defined gradient or random copolymerization. Macromolecules 40:3599–3609

41. Weber C, Hoogenboom R, Schubert US (2012) Temperature responsive bio-compatible polymers based on poly(ethylene-oxide) and poly(2-oxazoline)s. Prog Polym Sci 37:686–714

42. Park JS, Kataoka K (2006) Precise Control of lower critical solution temperature of thermosensitive poly(2-isopropyl-2-oxazoline) via gradient copolymerization with 2-ethyl-2-oxazoline as a hydrophilic comonomer. Macromolecules 39:6622–6630

43. Hoogenboom R, Thijs HML, Jochems M, van Lankvelt BM, Fijten MWM, Schubert US (2008) Tuning the LCST of poly(2-oxazoline) s by varying composition and molecular weight: alternatives to poly(N-isopropylacrylamide)? Chem Commun 5758–5760

44. Huber S, Hutter N, Jordan R (2008) Effect of end group polarity upon the lower critical solution temperature of poly(2-isopropyl-2-oxazoline). Colloid Polym Sci 286:1653–1661

45. Kempe K, Neuwirth T, Czaplewska J, Gottschaldt M, Hoogenboom R, Schubert US (2011) Poly(2-oxazoline) glycopolymers with tunable LCST behavior. Polym Chem 2:1737–1743

46. Ye X, Yang J, Ambreen J (2013) Scaling laws between hydrodynamic parameters and molecular weight of linear poly(2-ethyl-2-oxazoline). RSC Advances 3:15108-15113

47. Zhang N, Luxenhofer R, Jordan R (2012) Thermoresponsive poly(2-oxazoline) molecular brushes by living ionic polymerization: kinetic investigations of pendant chain grafting and cloud point modulation by backbone and side chain length variation. Macromol Chem Phys 213:973–981

48. Hoogenboom R, Fijten MWM, Schubert US (2004) Parallel kinetic investigation of 2-oxazoline polymerizations with different initiators as basis for designed copolymer synthesis. J Polym Sci A Polym Chem 42:1830–1840

49. Salzinger S, Huber S, Jaksch S, Busch P, Jordan R, Papadakis CM (2012) Aggregation behavior of thermo-responsive poly(2-oxazoline) s at the cloud point investigated by FCS and SANS. Colloid Polym Sci 290:385–400

50. Grillo I (2008) Small-Angle neutron scattering and applications in soft condensed matter. In: Borsali R, Pecora R (eds) Soft-matter characterization, vol 2. Springer

51. Teixeira J (1988) Small-angle scattering by fractal systems. J Appl Crystallogr 21:781–785

52. Ivanova R, Komenda T, Bonné TB, Lüdtke K, Mortensen K, Pranzas PK, Jordan R, Papadakis CM (2008) Micellar structures of hydrophilic/lipophilic and hydrophilic/fluorophilic poly(2-oxazoline) diblock copolymers in water. Macromol Chem Phys 209:2248–2258

53. de Gennes P-G (1979) Scaling concepts in polymer physics. Cornell University Press, Ithaca and London

54. Porod G (1951) Die Röntgenkleinwinkelstreuung von dichtgepackten kolloiden Systemen. Kolloid-Zeitschrift 124:83–114

55. Ruland W (1971) Small-angle scattering of 2-phase systems—determination and significance of systematic deviations from Porods Law. J Appl Crystallogr 4:70–73

56. Koberstein JT, Morra B, Stein RS (1980) Determination of diffuse-boundary thicknesses of polymers by small-angle X-ray-scattering. J Appl Crystallogr 13:34–45

57. Schmidt PW (1982) Interpretation of small-angle scattering curves proportional to a negative power of the scattering vector. J Appl Crystallogr 15:567–569

58. Kline SR (2006) Reduction and analysis of SANS and USANS data using IGOR Pro. J Appl Crystallogr 39:895–900

59. Schärtl W (2007) Light scattering from polymer solutions and nanoparticle dispersions. Springer, Heidelberg

60. Junk MJN, Li W, Schlüter AD, Wegner G, Spiess HW, Zhang A, Hinderberger D (2011) Formation of a mesoscopic skin barrier in mesoglobules of thermoresponsive polymers. J Am Chem Soc 133:10832–10838

61. Aseyev V, Hietala S, Laukkanen A, Nuopponen M, Confortini O, Du Prez FE, Tenhu H (2005) Mesoglobules of thermoresponsive polymers in dilute aqueous solutions above the LCST. Polymer 46:7118–7131

62. Wu C, Li W, Zhu XX (2004) Viscoelastic effect on the formation of mesoglobular phase in dilute solutions. Macromolecules 37:4989–4992

63. Matsuo ES, Tanaka T (1988) Kinetics of discontinuous volume phase-transition of gels. J Chem Phys 89:1695–1703